Effect of environment partitioning on the survival and coexistence of autocatalytic replicators

İnanç Birol*
Department of Chemical Engineering, Northwestern University, 2145 Sheridan Road, Evanston, Illinois 60208

Satish J. Parulekar† and Fouad Teymour‡
Department of Chemical and Environmental Engineering, Illinois Institute of Technology, 10 West 33rd Street, Room 127, Chicago, Illinois 60616

(Received 14 March 2002; published 26 November 2002)

The paradigm of cubic autocatalytic replicators with decay in coupled isothermal continuous stirred tank reactors is selected as a model to study complex behavior in population dynamics of sexually reproducing species in a heterogenous environment. It is shown that, even a setup with single species in two coupled environments may have regions in parameter space that result in chaotic behavior, hence segregation in the environment causes complexity in the system dynamics. Furthermore, partitioning is found to lead to emergence phenomena exemplified by steady states not obtainable in the equivalent homogeneous system. These phenomena are illustrated through case studies involving single or multiple species. Results show that the coupled environments can host species, that would not survive should the coupling be removed.

DOI: 10.1103/PhysRevE.66.051916 PACS number(s): 87.10.+e, 82.40.Bj, 89.60.−k

I. INTRODUCTION

Observed in their natural environment, most living species are found to exist in organized social settings reflecting various degrees of intermingling with other species. The prospects of survival and coexistence of these species in these environments is strongly impacted by the nature of the interactions between them and by the type of environment they populate. For example, on the large scale of the biosphere, a variety of living organisms play a primary role in completing the natural cycles of carbon, nitrogen, oxygen, and numerous other elements, thus performing a function that is critical to the sustenance of life itself. Even the smallest living species, microorganisms, while interacting in numerous ways with human activities, play a most prominent role in the completion of these elemental cycles. Rarely is any species found to live in total isolation, as mixed populations of organisms are obviously the rule rather than the exception in natural systems. The basic types of interactions between species in these mixed populations are mainly described as either (i) competition, (ii) mutualism, (iii) commensalism, (iv) neutralism, (v) amensalism, (vi) predation or (vii) parasitism [1,2]. Whenever one or more of these types of interactions are present in a communal environment, various facets of complex behavior are displayed by its inhabitants.

The theoretical study of the behavior of systems involving the interaction of populations of multiple species is achieved through the use of mathematical models based on different paradigms of population biology [3–14]. The interested reader may find a good elementary introduction to mathematical models of biology in the textbook by Edelstein-Keshet [15], and a thorough accounting of diverse aspects of mathematical biology in the textbook by Murray [16].

In a recent article, Birol and Teymour [17] studied competitive autocatalysis as a population biology paradigm. Their analysis focused on multiple species populating a continuous stirred tank reactor (CSTR) while competing for a resource R which is externally supplied to the reactor at a constant rate. In bacterial growth systems, experimental bifurcation studies show that, feed limitation can cause population cycles [18]. However, for sexually reproducing organisms, population cycles are generally attributed to species interactions, and are most popularly modeled through predator-prey dynamics [cf. Ref. [16]]. In Ref. [17], Birol and Teymour showed that, like bacterial growth systems, feed limitation can be the cause of population cycles, rather than species interactions. They furthermore showed that, as many as $(2^{n+1}-1)$ steady states can be found whenever n species are considered in the system, some of which correspond to multiple species configurations. However, they also provided proof that no steady state involving the coexistence of multiple species was stable. This result, apparently in contrast with the observation of biodiversity, has been commonly found in a multitude of other homogeneous, autonomous systems restricted to pure and simple competition as the single source of interaction among their inhabitants. This *competitive exclusion* principle [19], also known as the *plankton paradox* [20], raises questions about the sustainability of natural ecology in view of the human activities (aided by great mobility and an unsettling appetite for consumption) that disturb the Earth's ability to support biodiversity [21]. However, it is not uncommon to observe multiple living species in apparent competitive coexistence in natural situations, in spite of the competitive exclusion principle. Three major reasons are normally believed to contribute to this: (i) the fact that the environment could be spatially nonuniform, (ii) the possibility that the external influences are not time invariant, and (iii) the possibility that one or more types of interactions besides competition occur between the living species [22].

*Electronic address: biroli@northwestern.edu
†Electronic address: parulekar@iit.edu
‡Electronic address: teymour@iit.edu

The main objective of the present article is to explore the applicability of this hypothesis to the autocatalytic replicator system of Birol and Teymour [17], but only in as much as the ''spatial homogeneity'' assumption is concerned. To accomplish this task, we test the effect of internal partitioning on the behavior of the CSTR system, as we consider two coupled interacting CSTRs of the type illustrated in Fig. 1. The analysis will still utilize the cubic autocatalator [3–7,17,23,24],

$$R + 2P \xrightarrow{k} 3P \tag{1}$$

with catalyst decay,

$$P \xrightarrow{k_d} D \tag{2}$$

to model the population dynamics of any specific species living in this environment. Results will show that the stable coexistence of two distinct species is provided by this partitioned environment under a range of operating conditions, thus supporting the conjecture that partial segregation of the environment leads to a higher potential for biodiversity.

This system of two interacting coupled CSTRs can be viewed as an aggregation of two subsystems, each of which is equivalent to the original homogeneous CSTR. In this regard, it provides an additional interesting facet, as it displays the phenomenon of *emergence* featured by complexity theory [25]. Emergence, in this sense, refers to any situation in which a system displays a level of functionality that is not possible for any of its subsystems when considered on their own. The ability to support coexistent distinct species is obviously lacking from the homogeneous single CSTR system, but emerges as a generic capability of the coupled reactor system. Analysis will further show that emergence can also be observed even when a single species is considered in this system. Results will illustrate operating conditions under which the mere existence of this species in the homogeneous CSTR is impossible, yet that lead to thriving survival in the same environment, when partitioning is introduced.

II. COMPETITIVE EXCLUSION

A. Biological and ecological aspects

The validity and applicability of the so-called *survival of the fittest* phenomenon and the associated competitive exclusion principle have been the subject of debate among ecologists. Several experimental and theoretical studies [cf. [26] for references], have shown that competition of two populations for a single rate-limiting nutrient leads to extinction of one of the populations in a spatially uniform environment that is not subject to temporal variations in external influences. This pure and simple competition is the most widely studied type of interaction between species populations that inhabit a common environment. Generally, these interactions are broadly classified into two types, namely, indirect interactions (exerted through the abiotic environment) or direct interactions (involving direct physical contact of the interacting organisms) [27]. Regardless of whether a living species is unicellular or multicellular, its functioning and survival are dependent on processes occurring in each cell. The activity of each cell is a sum of thousands of molecular level chemical reactions occurring inside the cell which lead to utilization of resources to generate building blocks of cellular material and a host of other chemicals and are promoted by a large number of enzymes (biological catalysts). The progress of each reaction is strongly dependent on key variables such as pressure, temperature and pH. The ecosystem at large and any of its subsections (of whatever size, e.g., lakes, ponds, and rivers of different sizes, seas, and oceans) are characterized by substantial spatial and temporal variations in these key variables and other such variables. These spatial and temporal variations are responsible in part for the preservation of biodiversity. Humans have tried to mimic the functioning of living species in natural environments in ''controlled'' settings in research laboratories and industrial complexes. Even in these settings, spatial and temporal variations in key variables influencing the functioning of living species are increasingly common as the scale of operation is increased [28–30].

As mentioned, the overwhelming majority of studies revolving around the *competitive exclusion* principle involve the cellular population dynamics of microbial mixed cultures. The rate of reproduction of cells in these cultures is often expressed according to kinetics of the Michaelis-Menten type (which are analogous to the Langmuir-Hinshelwood type rate expressions used for chemical catalytic reactions) [31]. In these, the specific growth rate of the cellular population μ is governed by the Monod equation [32], which approaches a linear dependence on the resource at low resource concentration and saturates to a maximum growth rate $\mu_{\max}$ at higher levels. A plethora of variations on this basic rate equation have been proposed in the literature for rates of cell replication [see Refs. [1,33] and [34] for several examples of these]. In some of these variations, the order of reaction with respect to resources is less than unity and with respect to end-products is nonpositive (not surprising since synthesis of building blocks for cellular material and synthesis of end products are competing processes as concerns utilization of nutrient and energy sources within the living species).

The apparent discrepancy between the common observance of biodiversity in nature and the findings of studies on the dynamics of mixed cultures has long been believed to be attributable to spatial inhomogeneities and/or temporal variations in inputs. Both of these hypotheses have been confirmed in further studies. Using the well-known Monod kinetics for describing growth of two competing microbial populations, it has been established theoretically that the two competing populations can be sustained in a controlled laboratory environment by periodic variations in feed conditions to a continuous culture in a well mixed CSTR or by introducing spatial inhomogeneity in the culture by considering two or more CSTRs with two-way exchange of the culture between them [26,35–37].

Another major source of deviation from competitive exclusion could be the type of interaction between the two populations living in the environment. The closest type to pure and simple competition is commensalism, in which a commensal population benefits from a host population via a unidirectional interaction. Mixed cultures exhibiting commensalism with/without competition play an instrumental role in ecology, in many commercial biological production processes, and in environmental cleanup and remediation processes. Even in spatially uniform environments and under time-invariant external influences, these populations exhibit rich behavioral patterns [38,39]. Genetic engineering techniques have opened new avenues for enhanced production of many valuable biochemicals, and discovery and synthesis of new biochemicals. While the use of extrachromosomal DNA vectors (such as plasmids) allows for overproduction of the target vector-encoded metabolites, reversion of the recombinant cells (host population) to vector-free cells (commensal population) at cell division due to loss of all vector (e.g., plasmid) copies and the significant growth advantage that the commensal population has over the host population (competition for common nutrients) places limitations on sustained production of the target metabolites. Dominance of the unproductive vector-free cells can usually be obviated by applying a selection pressure, such as an antibiotic. Insertion of the antibiotic marker gene in the DNA vector renders immunity for recombinant cells from the antibiotic, while the antibiotic leads to death of or repression of growth of vector-free cells. Supplying appropriate amounts of antibiotic ensures retention of recombinant population in the mixed culture. The *emergence* phenomenon to be discussed later in this work has been demonstrated for these mixed cultures by periodic need-based addition of antibiotic [40]. Another example of mixed cultures (populations) is the healthy cells and cancerous cells in animal tissue and blood. The cancerous cells (commensal population) are generated from healthy cells (host population) and have significant growth advantage over healthy cells (competition for common nutrients and energy resources). Survival of healthy cells then depends on application of appropriate selection pressure (such as chemotherapy and radiation treatment) to suppress as much as possible the growth (spreading) of cancerous cells. One should recognize that these last two examples of populations with commensalistic interaction involve both direct and indirect interaction.

It should also be noted that any given species would be protected from competitive exclusion whenever it is being continuously introduced into the system through its feed stream, even if in trace amounts. Any such species would acquire robustness against extinction from the parameter space of the system by virtue of the fact that it can always recover to healthy population levels when conditions are suitable [41,42]. This situation, for example, might be encountered in the dynamics of fish populations in a body of water where periodic restocking is practiced by the Department of Natural Resources (DNR).

B. Applicability to autocatalytic replicators

The present study utilizes a paradigm for population dynamics based on the cubic autocatalator described by Eqs. (1) and (2). As noted by Birol and Teymour [17], this is best analogous to sexual reproduction in higher macroorganisms. They also note however that the closely related quadratic autocatalysis is an alternative paradigm for asexual reproduction by cell division, since only 1 mole of P participates in the reaction instead of 2. It is worthy of note that their analysis proves that competitive exclusion is also found in homogeneous, autonomous autocatalytic competition, thus indicating that this principle is not affected by the mode of replication in action. This proof was presented in Ref. [17] for steady state coexistence and will be extended here to prove the lack of long term dynamic coexistence.

Theorem 1.: Impossibility of indefinite coexistence. In a dynamical system of N cubic autocatalytic species in a single homogeneous isothermal CSTR with constant resource feed, more than one species cannot have a stable coexistence.

Proof 1. Let us start by writing the model equations for the system. A material balance on the resource concentration R and each of the species concentrations P_i yields

$$V\frac{dR}{dt'} = -\sum_{i=1}^{N} Vk_i R P_i^2 + F(R_0 - R), \tag{3}$$

$$V\frac{dP_i}{dt'} = Vk_i R P_i^2 - (Vk_{di} + F)P_i, \tag{4}$$

where t' represents the time, F is the volumetric flow rate, R_0 is the feed concentration of resource, k_i and k_{di} are the reproduction and death rates for species i, respectively. We can modify the model equations, by defining $r = R/R_0$, $p_i = P_i/R_0$, $t = R_0^2 t'$, $f = F/(VR_0^2)$, and $d_i = k_{di}/R_0^2$, thus yielding the dimensionless model equations,

$$\frac{dr}{dt} = -\sum_{i=1}^{N} k_i r p_i^2 + f(1-r), \tag{5}$$

$$\frac{dp_i}{dt} = k_i r p_i^2 - (d_i + f)p_i. \tag{6}$$

We can use the model equations (5) and (6) and the time derivative of $r + \Sigma_i p_i$,

$$\frac{d}{dt}\left(r + \sum_i p_i\right) = f\left(1 - r - \sum_i p_i\right) - \sum_i d_i p_i \tag{7}$$

to deduce the following constraints on concentrations:

(i) $r(t) > 0$ for all physically meaningful cases, and after the transients vanish, $0 < r(t) \leqslant 1$.

(ii) Again, after the transients, $r(t) + \Sigma_i p_i(t) \leqslant 1$, which implies $\forall i$, $p_i(t) < 1$.

(iii) If $p_i(\infty) \neq 0$, then $p_i(t) > (d_i + f)/k_i$.

From the last two constraints, we can write if $1 < (d_i + f)/k_i$, then $p_i(\infty) = 0$.

Note that, considering the dynamics of the reciprocal of the species concentrations, $s_i(t) = 1/p_i(t)$, we obtain a set of linear differential equations for $s_i(t)$, with $r(t)$ being the forcing function, given as

$$\frac{ds_i}{dt} = -k_i r + (d_i + f)s_i . \tag{8}$$

Assume that we are investigating the system after the transients are settled, and all $s_i(t)$, $i=1,\ldots,N$, are finite, which, following the above constraints, means

$$1 < s_i(t) < \frac{k_i}{d_i + f}, \quad \forall i. \tag{9}$$

Since coexistence steady states of this system are always unstable [17], the system is to have a limit set.

Next, let us write the Jacobian matrix of the system in the $(r, s_1, s_2, \ldots, s_N)$ space,

$$J = \begin{bmatrix} -\sum_i k_i/s_i^2 - f & 2k_1 r/s_1^3 & 2k_2 r/s_2^3 & \ldots & 2k_N r/s_N^3 \\ -k_1 & d_1 + f & 0 & \ldots & 0 \\ -k_2 & 0 & d_2 + f & \ldots & 0 \\ \vdots & \vdots & \vdots & & \vdots \\ -k_N & 0 & 0 & \ldots & d_N + f \end{bmatrix} \tag{10}$$

along the trajectory, and find its eigenvalues to determine the orbital stability of this limit set.

The characteristic polynomial of the system can be written in a compact form as

$$|\lambda I - J| = \sum_{i=1}^{N} \left\{ \left[\frac{\lambda^2}{N} + \lambda\left(\frac{k_i}{s_i^2} - \frac{d_i}{N} \right) + \frac{2k_i^2 r}{s_i^3} - (d_i + f)\left(\frac{k_i}{s_i^2} + \frac{f}{N} \right) \right] \prod_{j \neq i} (\lambda - d_j - f) \right\}. \tag{11}$$

Note that, for a single-species system ($N=1$), the stability of the orbit depends on the choice of the system parameters, as well as the initial conditions. Indeed, the single-species system does have stable and unstable steady states and limit cycles [17].

For an N-species system, with $N>1$, the characteristic polynomial, $P_{N+1}(\lambda)$ defined in Eq. (11) is the sum of N polynomials, $P^i_{N+1}(\lambda)$, $i=1,\ldots,N$, each with at least $(N-1)$ real-positive roots at $\lambda_j = d_j + f$ with $j \neq i$. Without loss of generality, assume that d_i's are sorted in decreasing order. Investigating the sign of $P_{N+1}(\lambda)$ at $\lambda_1 = d_1 + f$ and $\lambda_2 = d_2 + f$,

$$P_{N+1}(\lambda_1) = \frac{2k_1^2 r}{s_1^3} \prod_{i \neq 1} (d_1 - d_i) > 0, \tag{12}$$

$$P_{N+1}(\lambda_2) = \frac{2k_2^2 r}{s_2^3} \prod_{i \neq 2} (d_2 - d_i) < 0, \tag{13}$$

we conclude that, $P_{N+1}(\lambda)$ has a real-positive root in the range $(d_2 + f, d_1 + f)$. Following the same line of thought, we can deduce that, there are $(N-1)$ real-positive roots in the range $(d_N + f, d_1 + f)$. This implies that, if the orbit defines an attractor, we can compute the Lyapunov exponents along that, to find $(N-1)$ positive Lyapunov exponents, since there are at least $(N-1)$ mutually orthogonal directions along which close-by orbits diverge. Furthermore, if our system is orbiting on an attractor, it cannot have more than $(N-1)$ positive Lyapunov exponents. The remaining two should be composed of a zero and a negative Lyapunov exponent with a magnitude greater than the sum of the positive exponents. Since the conditions thus set for an attractor (if and when it exists) are valid for the whole parameter space, this multiple species setup cannot have a stable limit cycle, but only a chaotic attractor (a hyperchaotic one, for $N>2$), if any. However, all established routes to chaos require a stable limit cycle to allow the transition [cf. Ref. [43]]. Also note that the absence of stable periodic attractors in the multispecies system rules out the common signatures of chaotic regimes of periodic windows and odd-period limit cycles, as well as orbits of infinite period (homoclinic and heteroclinic).

We can visualize the dynamic behavior of the system as follows. We have seen that, everywhere on the orbit, there are at least $(N-1)$ directions along which a small perturbation would grow locally exponentially in time. Such an ejection from the orbit would never make it back along a contraction direction, but eventually defy the bounds set by the inequality (9), and the multispecies setup will collapse into either a single-species setup or into total extinction. Mathematically speaking, we can implicitly integrate Eq. (8) for species i and j to get

$$\frac{s_i(t)}{k_i} - \frac{s_j(t)}{k_j} = \frac{s_i(0)}{k_i} e^{(d_i+f)t} - \frac{s_j(0)}{k_j} e^{(d_j+f)t} - \int_0^t r(\tau)\left(e^{(d_i+f)(t-\tau)} - e^{(d_j+f)(t-\tau)}\right) d\tau. \tag{14}$$

Note that, when $d_i \neq d_j$, and $t \to \infty$, the right hand side of this equation will be dominated by the expressions of the species with larger death rate. For instance, if $d_i > d_j$, then

$$\lim_{t\to\infty} \frac{s_i(t)}{k_i} - \frac{s_j(t)}{k_j} = \lim_{t\to\infty} \frac{s_i(t)}{k_i}. \tag{15}$$

The only possible way that this could happen is by $s_i \to \infty$, hence the species i goes extinct.

In the special case of $d_i = d_j$, we can write

$$\frac{s_i(t)}{k_i} - \frac{s_j(t)}{k_j} = \left(\frac{s_i(0)}{k_i} - \frac{s_j(0)}{k_j} \right) e^{(d_i+f)t} \tag{16}$$

which would diverge to plus or minus infinity when $s_i(0)/k_i \neq s_j(0)/k_j$. If we consider an initial condition $s_i(0)/k_i = s_j(0)/k_j$ in this special case, then the motion will be trapped to the $s_i(t)/k_i = s_j(t)/k_j$ manifold, which we have shown above to be unstable. An example of the latter case was presented in Ref. [17].

As a result, multiple species cannot have stable coexistence in this system. ■

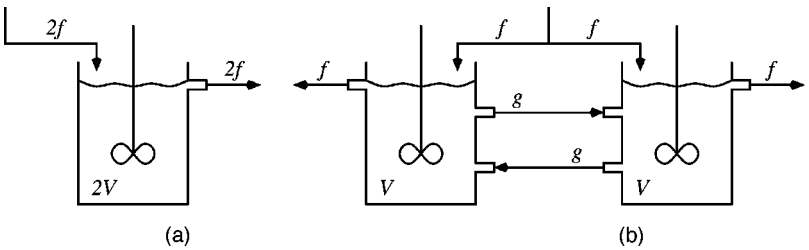

FIG. 1. (a) A homogeneous CSTR. (b) Equal partitioning of the CSTR in (a) as two coupled CSTRs.

III. SINGLE SPECIES IN TWO CSTRs

Prior to our analysis of the two-species problem in Sec. IV, we will focus our study in this section on the behavior of a single species, when allowed to populate the coupled CSTR system. Variants of this problem have been studied by Kim and Hlavacek [44], and Taylor and Kevrekidis [45,46], but were limited to the study of resonance phenomena, quasiperiodicity and chaotic dynamics resulting from the coupling of oscillators. In this article we will analyze this single-species system with the aim of exploring the base upon which the parameter space of the two-species problem is built, and of presenting another example of emergent phenomena in complex systems. The latter is illustrated by the ability of the coupled system to sustain the species under conditions that result in total washout in the equivalent homogeneous CSTR. Although the focus of our analysis will be on the analysis of the steady state bifurcation structure, we will present dynamic results that exhibit chaotic flows produced via the quasiperiodicity route, thus in agreement with the findings of Taylor and Kevrekidis [45,46].

The system of two isothermal CSTRs with constant feed of resource of concentration R_0, and feed rate F, that host populations of concentration P_i, $i=1,2$, which reproduce sexually and decay with reactions of Eqs. (1) and (2), respectively, is illustrated in Fig. 1(b). Let the concentration of resource in reactor i be shown by R_i, and the interaction be characterized by the flow rate G. If we operate the two reactors at a constant and equal volume V, we can write the model equations governing the resource and population balance as

$$V\frac{dR_i}{dt'} = -VkR_iP_i^2 + F(R_0 - R_i) + G(R_{i'} - R_i), \quad (17)$$

$$V\frac{dP_i}{dt'} = VkR_iP_i^2 - (F + Vk_d)P_i + G(P_{i'} - P_i), \quad (18)$$

where t' represents time, and i' *the other* reactor, i.e., if $i=1$, then $i'=2$ and vice versa. If we define the dimensionless concentrations $r_i = R_i/R_0$ and $p_i = P_i/R_0$, scale the time $t = t'R_0^2$, and define new parameters $d = k_d/R_0^2$, $f = F/(VR_0^2)$ and $g = G/(VR_0^2)$, then the model equations become

$$\frac{dr_i}{dt} = -kr_ip_i^2 + f(1 - r_i) + g(r_{i'} - r_i), \quad (19)$$

$$\frac{dp_i}{dt} = kr_ip_i^2 - (f + d)p_i + g(p_{i'} - p_i). \quad (20)$$

Although in this setup, we may further scale time to get rid of the reproduction rate k in favor of reducing redundancy, we will keep it, for the sake of notational consistency with Sec. IV, where we investigate the two-species case.

The coupling strength is characterized by the dimensionless interaction flow rate g. In the absence of coupling, $g=0$, we naturally will have two isolated CSTRs equivalent to the original CSTR. At the other extreme as $g \to \infty$, the fast rate of interchange will tend to equalize the concentrations of R and P in both reactors, making them again indistinguishable from a single large homogeneous CSTR [Fig. 1(a)]. The feed rate f will be doubled for the latter, but so will be the volume. The effect of the external feed rate f is different. If we do not feed the system sufficiently, ($f \to 0$,) the population will starve to death, as there will not be enough resources to consume for reproduction. At the other extreme, if we feed the system too much, ($f \to \infty$,) the residence time in the system will tend to zero, and the species will not have any foothold in the system. Therefore, there is a finite region in the f parameter space, that would host a population of species P, subject to the condition $k/d > 16$ [17].

A. Static complexity

Being a nonlinear system, a cubic autocatalator enjoys multistability, and we will start this section by enumerating possible steady states, using the four equilibrium equations

$$-kr_ip_i^2 + f(1 - r_i) + g(r_{i'} - r_i) = 0, \quad (21)$$

$$kr_ip_i^2 - (f + d)p_i + g(p_{i'} - p_i) = 0, \quad (22)$$

where $i=1,2$ and $i' \neq i$ as before.

First of all, as in the single CSTR case, if no species is populating the environment, $p_i = 0$, the fed resources will not be consumed, and $r_i = 1$. Thus the trivial steady state of this system is

$$\mathrm{SS0} = (r_i = 1, p_i = 0). \quad (23)$$

It can be readily shown that this steady state is always stable.

Next, let us consider the symmetric solutions for this system of equations, where $p_1 = p_2$ and $r_1 = r_2$, which are clearly equivalent to the equilibrium equations of a single CSTR

$$-kr_ip_i^2 + f(1 - r_i) = 0, \quad (24)$$

$$kr_i p_i^2 - (f+d)p_i = 0. \tag{25}$$

In Ref. [17] the steady states of a single CSTR were found to be given by

$$\mathrm{SS1} = \left(r_i = \frac{1+\sqrt{\Delta}}{2}, p_i = \frac{f(1-\sqrt{\Delta})}{2(f+d)} \right), \tag{26}$$

$$\mathrm{SS2} = \left(r_i = \frac{1-\sqrt{\Delta}}{2}, p_i = \frac{f(1+\sqrt{\Delta})}{2(f+d)} \right), \tag{27}$$

where

$$\Delta = 1 - \frac{4(f+d)^2}{kf}. \tag{28}$$

Note that SS1 and SS2 exist only when $\Delta > 0$, which corresponds to a finite range in $f \in (f_-, f_+)$, where

$$f_\pm = \frac{1}{8}(k - 8d \pm \sqrt{k}\sqrt{k-16d}), \tag{29}$$

and such a range exists only if $k/d > 16$. The analysis also showed that SS1 is always unstable, and that SS2 is stable for $f \in (f_H, f_+)$, where

$$f_H = \frac{2d}{(k/d)^{1/2} - 2 + (k/d - 4(k/d)^{1/2})^{1/2}} \tag{30}$$

is the feed rate at which the system experiences a Hopf bifurcation. In the range $f \in (f_-, f_H)$, SS2 is unstable.

Theorem 2: Conservation of stability structure for single-CSTR steady states. The stability structure of the steady states of each of two identical uncoupled CSTRs, as defined by Eqs. (24) and (25) is conserved, when these are coupled by an interaction flow rate, g.

Proof 2. Note that the Jacobian matrix of the coupled CSTRs hosting a single species

$$A = \begin{bmatrix} -kp_1^2 - f - g & -2kr_1p_1 & g & 0 \\ kp_1^2 & 2kr_1p_1 - f - d - g & 0 & g \\ g & 0 & -kp_2^2 - f - g & -2kr_2p_2 \\ 0 & g & kp_2^2 & 2kr_2p_2 - f - d - g \end{bmatrix} \tag{31}$$

is in the form

$$A = \begin{bmatrix} A_1 - gI & gI \\ gI & A_2 - gI \end{bmatrix}, \tag{32}$$

where I is the 2×2 identity matrix, and

$$A_i = \begin{bmatrix} -kp_i^2 - f & -2kr_ip_i \\ kp_i^2 & 2kr_ip_i - f - d \end{bmatrix} \tag{33}$$

for the steady state values of r_i and p_i. If the two CSTRs have identical steady states, $A_1 = A_2$, and the Jacobian matrix A can be transformed to

$$\hat{A} = \begin{bmatrix} A_1 & 0 \\ 3gI & A_1 - 2gI \end{bmatrix} \tag{34}$$

using the similarity transformation, $\hat{A} = S^{-1}AS$ with

$$S = \begin{bmatrix} 2I & -I \\ -I & I \end{bmatrix}. \tag{35}$$

Therefore the characteristic equation can be written as

$$|\lambda I - A| = |\lambda I - A_1||(\lambda + 2g)I - A_1| = 0, \tag{36}$$

and will have right half plane eigenvalues, if and only if A_1 does. Note that, this property can easily be further generalized to multiple-species steady states in two identical CSTRs. ■

Up to here, we have shown that the single-CSTR steady states and their stability structure are valid for the coupled system. Now let us consider two decoupled CSTRs, each at one of its three steady states, and couple them, by slowly increasing the interaction flow rate. As we have shown, if both start at the same steady state, nothing will change and the single-CSTR steady states will prevail for any g. However, if they start from two different steady states, in accordance with the implicit function theorem, the new steady state of the coupled system will be a continuous deformation of the decoupled steady states in the limit of small interaction flow rates, g. As a result, additional steady states will be observed. Eventually, as g exceeds a certain threshold, the deformed steady states will disappear, since for *large enough* g, we will approach the single-CSTR limit. Hence, in the coupled system, we will have at most nine steady states, three of them being the single-CSTR steady states, and six of them developing because of the coupling. The six new steady states come from the roots of a sixth order polynomial. After manipulating the steady state equations using Maple software [47], we can express that polynomial in p_1, with coefficients

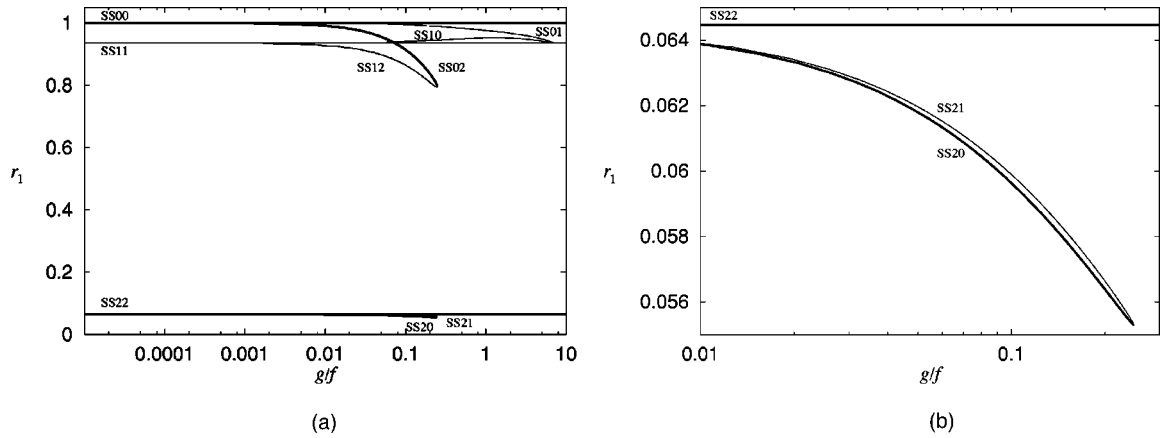

FIG. 2. Steady states for r_1 in the coupled CSTRs with $f=0.0077$, hosting a species with $k=25$ and $d=0.1$. The bifurcation parameter is the interaction flow rate, g. (a) Nine steady states of the system system are marked. (b) A closeup of the bifurcation diagram showing SS20, SS21, and SS22.

$$p_1^6/+k^3(f+2g+d)(f^2+2fg+df+dg)^2,$$

$$p_1^5/-2fk^3(f+2g)(f+2g+d)(f^2+2fg+df+dg),$$

$$p_1^4/+k^2(f+2g)(f+2g+d)$$
$$(2f^4+7f^3g+f^3k+4f^3d+2f^2d^2+6f^2g^2$$
$$+10f^2dg+2f^2kg+3fgd^2+4g^2df+g^2d^2),$$

$$p_1^3/-fk^2(f+2g)^2(f+2g+d)(4fg+dg+2f^2+2df), \quad (37)$$

$$p_1^2/+kf(f+2g)^2$$
$$(f^4+5f^3g+3f^3d+f^2kg+11f^2dg+3f^2d^2+9f^2g^2$$
$$+7fgd^2+fd^3+2fkg^2+11g^2df+6fg^3+d^3g+2g^2d^2),$$

$$p_1^1/-f^2kg(f+2g)^3(f+2g+d),$$

$$p_1^0/+f^2g^2(f+2g)^3(f+2g+d).$$

Note the alternating sign of the coefficients of p_1^j, which is a necessary condition for $\Re\{p_1\}>0$ for all k, d, f, and $g \in \mathcal{R}^+$.

Let us label the new steady states by SSab, where a and b denote the combination of decoupled steady states that lead to it. For instance

$$\text{SS01}=\left(r_1=1,p_1=0;r_2=\frac{1+\sqrt{\Delta}}{2},p_2=\frac{f(1-\sqrt{\Delta})}{2(f+d)}\right) \quad (38)$$

at the branching point of $g=0$. Of course, when the system is at a steady state SSab from the reference frame of one reactor, it should be at the symmetric steady state SSba from the reference frame of the other reactor since they are identical. Thus, the stability structure of the steady states is symmetric in the indices a and b for this parametrization.

Example 1: Development of new steady states. Consider the two CSTRs of Fig. 1 and a population of species P with reproduction rate $k=25$ and death rate $d=0.1$, fed by a volumetric flow rate $f=0.0077$. The single CSTR steady states for this system are

$$\text{SS00}=(r_1=1,p_1=0;r_2=1,p_2=0), \quad (39)$$

$$\text{SS11}=(r_1=0.9355,p_1=0.0046;r_2=0.9355,p_2=0.0046), \quad (40)$$

$$\text{SS22}=(r_1=0.0645,p_1=0.0668;r_2=0.0645,p_2=0.0668). \quad (41)$$

Now, let us plot the bifurcation diagram for this system, using the content software [48], and the interaction flow rate g as the bifurcation parameter. If we start with these steady states and increase the interaction flow rate g we will observe the horizontal lines in the bifurcation diagram of Fig. 2(a). However, e.g., initial conditions combining (r_1,p_1) of SS0, and (r_2,p_2) of SS1, will yield the top curve emerging from $r_1=1$ in the first CSTR, and the curve that emerges from the top of $r_2=0.9355$ in the second. Note that, as argued above, the newly emerging steady states survive up to a certain threshold value of g, and disappear beyond that. There are six new steady states due to coupling. The pair of steady states below the line $r_1=0.0645$ are SS20 and SS21. The thick (thin) curves correspond to stable (unstable) steady states. For the parameter set of this example, SS2 is stable as well as SS0, and the new steady states SS02 and SS20 pairings have regions of stability. All the other pairings have at least one of the CSTRs at an unstable steady state, and the new steady states are unstable too, but this does not imply that new steady states should inherit the stability structure from their parent steady states. In Fig. 2(b), we have shown a closeup of the two steady states that emerge from SS22, to clarify their stability structure.

Note that, in this projection of the bifurcation diagram, SS02, crosses over SS11, and the three steady states SS01, SS10 and SS11 meet for a specific interaction flow rate. Although the first phenomenon is an artifact of projection, the latter is a result of the presence of a branching point, at $g=0.0533$.

We may generalize the enumeration scheme for the number of possible steady states to k mutually interacting CSTRs with a single autocatalytic species. In each reaction, for the $g \to 0$ limit, there are three possible steady states, thus 3^k possible configurations. When we let a configuration of CSTRs interact, by increasing the interaction flow rate, again according to the implicit function theorem, all 3^k distinct steady states will survive for a range of interaction parameter g, and then the bifurcation diagram will evolve into the three steady states of the $g \to \infty$ limit.

In this section, so far we argued the mechanism that results in new steady states due to coupling. Namely, we started with an asymmetric steady states configuration in decoupled CSTRs, and brought them together to observe the new steady states. It should be noted however that, coupled autocatalytic reactors have steady states that cannot be reached through this scheme. That is, even if the decoupled CSTRs do not have steady states for the operating parameters, the coupled system may. We can find those new steady states by using two-parameter continuation studies on the limit points and branching points of the asymmetric steady states.

Example 2: Emergence. Consider the system of example 1, operating at a feed rate of $f = 0.000\,977$. Note that SS1 and SS2 exist only for $f \in (0.001\,65, 6.0483)$. Therefore, the decoupled system has the trivial steady state of extinction only. However, the coupled system can have up to four nontrivial steady states, as shown in Fig. 3(a). Figure 3 shows the evolution of the bifurcation diagram r_1 versus g/f, and how those emerging steady states are related to the ''asymmetric steady states'' setup. The emerging steady states first materialize as two points in the $(r_1, g/f)$ plane and grow into distinct isolas [Fig. 3(a)]. As f is increased, they first come in contact, then intertwine [Fig. 3(b)] in this projection. Next they elongate towards $g = 0$, in anticipation of the limit of sustainability in a single CSTR, the upper isola touching the trivial steady state at $r_1 = 1$, and the other one touching $r_1 = 0.5$ [Fig. 3(c)] for $f = 0.001\,65$. At this value of f, the isolas are about to break at their touching point, then move apart, as the steady states of the single-CSTR materialize in this setup [Fig. 3(d)]. By increasing f, the branching points of SS12, SS22, SS21 triplet and SS02, SS22, SS20 triplet grow closer. After they meet, SS02 pairs up with SS12, and SS20 with SS21, and break from SS22 [Fig. 3(e)]. Thus, two distinct branching points evolve into two identical limit points. On the other hand, SS01 and SS10 do not undergo any fundamental changes throughout these transitions. Starting at Fig. 3(f), stability starts developing on SS02 and SS20 (shown by darker lines), where SS22 is also stable. As the gap between SS11 and SS22 grows wider, SS02, SS12 pair gets more and more confined between SS00 and SS11 [Figs. 3(f) and 3(g)]. When this gap starts shrinking again, by increasing f, the asymmetric steady states survive higher and higher interaction flow rates [Fig. 3(h)], until SS11 meets with SS22 at $r_1 = 0.5$, for $f = 6.0483$, where SS12 and SS21 become one.

A cross section of this behavior is better illustrated by the bifurcation diagram of Fig. 4, where the bifurcation parameter is the feed rate f and g is fixed at 0.002. The circular isola represents the nontrivial steady states of the decoupled system, and the amorphous isola is due to the coupling. If we label the steady states, at $f = 0.005$ from top to bottom, they are SS00, SS01, SS10, SS11, SS02, SS12, SS22, SS21, and SS20. Note that around $f \simeq 0.0075$, SS02, SS12, SS21, and SS20 disappear at the tips of the crescent, and do not appear until $f \simeq 0.3$.

An important fact in this bifurcation diagram of Fig. 4, in agreement with Figs. 3(a) and 3(b) is that, the domain of the amorphous isola on the f-axis exceeds that of the circular isola. Thus, coupling makes it possible for the species to have nontrivial steady states in the system, expanding the *space of possible*.

In an ecological analogy, consider, say a group of primates, living in an isolated environment with a scant flow of resources such that the group cannot survive under given conditions. If the group, however divides into two and forms territorial tribes, allowing only *controlled* interaction (in terms of population and resource interchange) they can stabilize the unstable emergence steady states and survive in that environment. In fact, such a territorial grouping is not uncommon among many species, and the phenomenon is explained in two schools of thought: *the predation school* and *the bully school*. The predation school claims that group living serves as predator control, both in the sense of easier detection of the predator, and lower probability of being the victim. In her study of black macaques on the Sulawesi island of Indonesia, Kinnaird observes that, although the macaque population on the island does not have a profound predator, they still live in social groups, and concludes that the bully school of thought should be the correct reasoning [49]. As suggested by our analysis, grouping may as well be the result of the underlying population dynamics.

Also, note that, not only do SS02 and SS20 have a range of f, where they represent stable steady states, with SS2 unstable, but the system can sustain a higher concentration of P as well in one of the CSTRs than it can have, if the CSTRs were decoupled. It may be possible to explain this emergence of stability by local fluctuations of the asymmetric system, that temporarily changes the effective volume and the residence time of each CSTR, thus bringing spatial inhomogeneity to the system.

Figure 5 illustrates how the bifurcation diagram of r_1 versus f evolves for changing g, further clarifying the conditions for the emergence phenomenon. In Fig. 5(a) the bifurcation diagram of the decoupled CSTRs is presented. It consists of the trivial solution line $r_1 = 1$ (not shown), and an isola which has a region of stable steady states, indicated by a darker portion on the lower right-hand corner of the diagram. In Figs. 5(b)–5(l), we deliberately omitted the isola of the decoupled case, in order not to obscure the asymmetric steady states. As we increase the interaction flow rate g the asymmetric steady states emanate in the vicinity of SS00, SS11, and SS22. We first observe an isola between SS00 and SS11, and two nested isolas near the isola of SS11 and SS22 [Fig. 5(b)]. Note that, the new steady states SS02 and SS20 have a region of stability. Then, as the interaction flow rate is increased, the top isola formed by SS10 and SS02 grows bigger while the other two new isolas get distorted [Fig. 5(c)], and after the top isola touches the inner isolas [Fig.

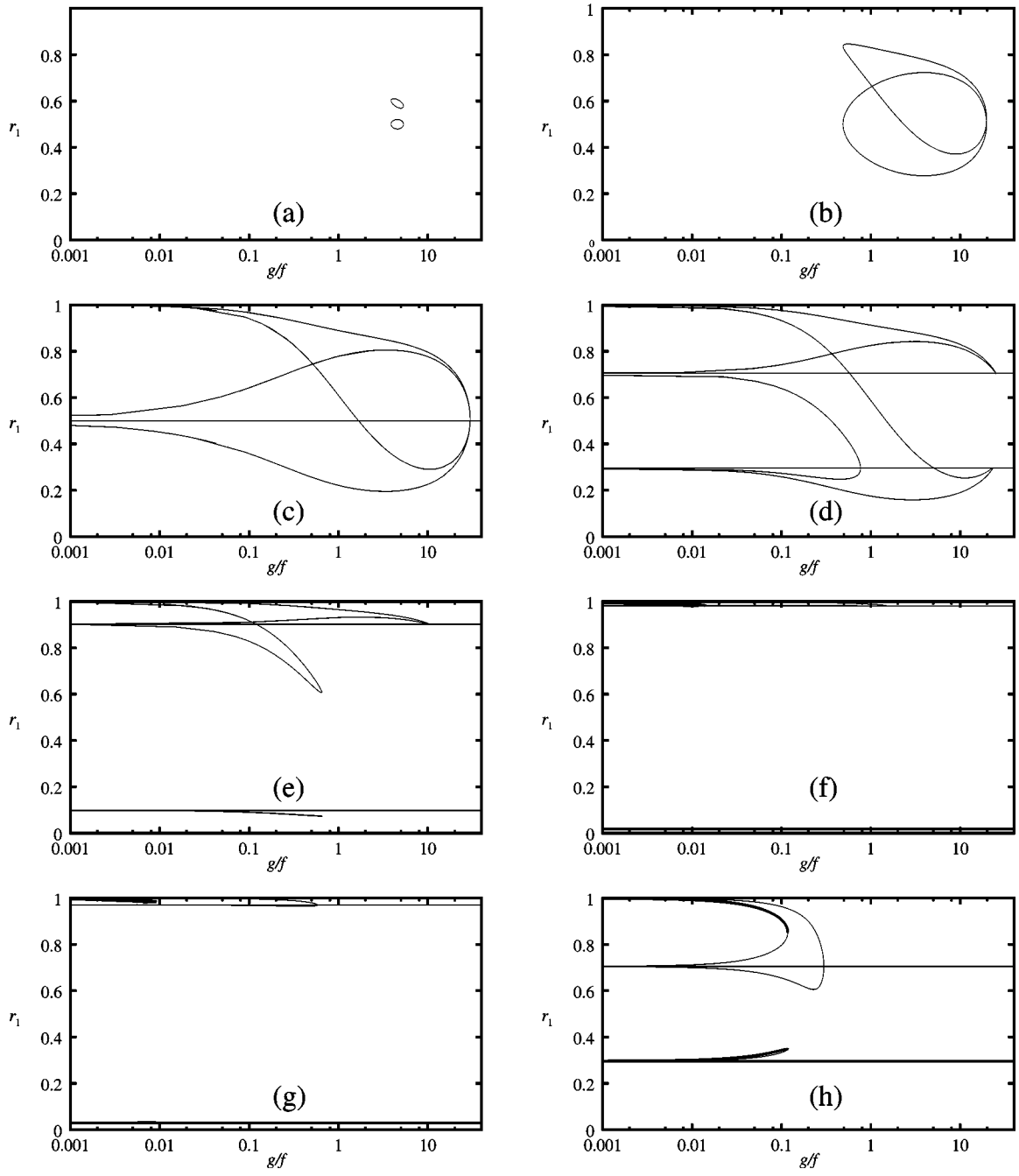

FIG. 3. Evolution of the bifurcation diagram of r_1 versus g/f in the coupled CSTRs for changing f [Eqs. (21) and (22)] hosting a species with $k=25$ and $d=0.1$. Feed rate is (a) 0.000 977, (b) 0.001 25, (c) 0.001 65, (d) 0.002, (e) 0.005, (f) 0.05, (g) 0.5, and (h) 5. The trivial steady state where $r_1=1$ is not shown. The horizontal lines stand for the steady states of the decoupled CSTRs which prevail in the coupled case.

5(d)] the three merge to form a single closed curve [Fig. 5(e)]. That is when SS02 and SS20 develop another region of stability located at the tips of the curve for lower f values. The stability regions on SS02 and SS20 enlarge the boundaries of survival for the species, thus, we again encounter an emergence phenomenon. This new region of stability shrinks with increasing g [Fig. 5(f)] and disappears [Fig. 5(g)] as the closed curve evolves towards a crescentlike shape [Fig. 5(h) and 5(i)]. Yet, even in Fig. 5(j), we have a twist in the curve, which eventually disappears in Fig. 5(k), at the cost of losing the lower tip of the crescent. As we further increase the interaction flow rate the closed curve shrinks further [Fig. 5(l)], then disappears. As we had argued earlier, beyond a certain threshold interaction flow rate, the bifurcation diagram of the coupled CSTRs is the same as that of the decoupled CSTRs.

The behavior of the limit points and the branching points of Figs. 3 and 5 can be summarized in a two-parameter continuation diagram (Fig. 6). The horizontal dark lines in the figure are the limit points of the single-CSTR system, showing the boundaries of the species isola. The dark curve be-

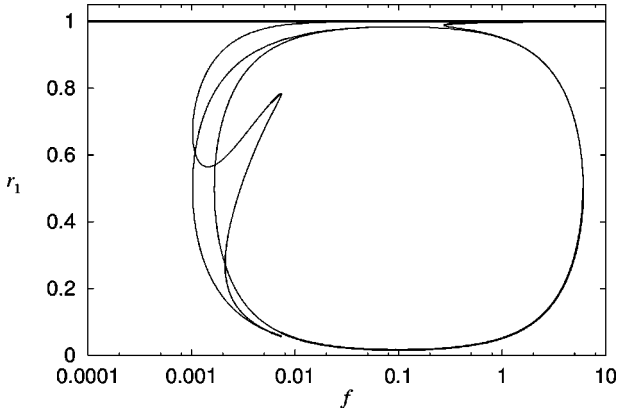

FIG. 4. Steady states for r_1 in the coupled CSTRs with $g=0.002$, hosting a species with $k=25$ and $d=0.1$. The bifurcation parameter is f.

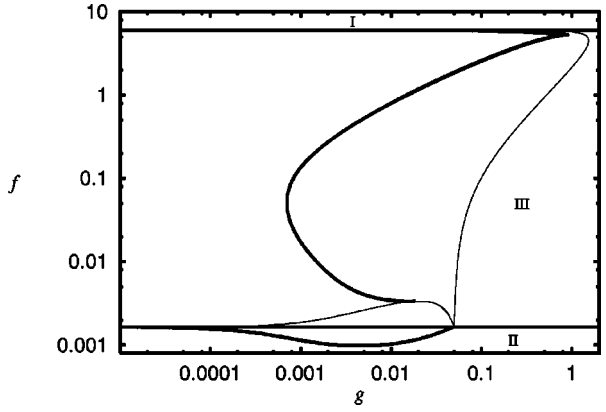

FIG. 6. Two parameter continuation diagram for the limit points and branching points for the CSTR hosting a species with $k=25$ and $d=0.1$. The dark lines show limit points and the light lines the branching points.

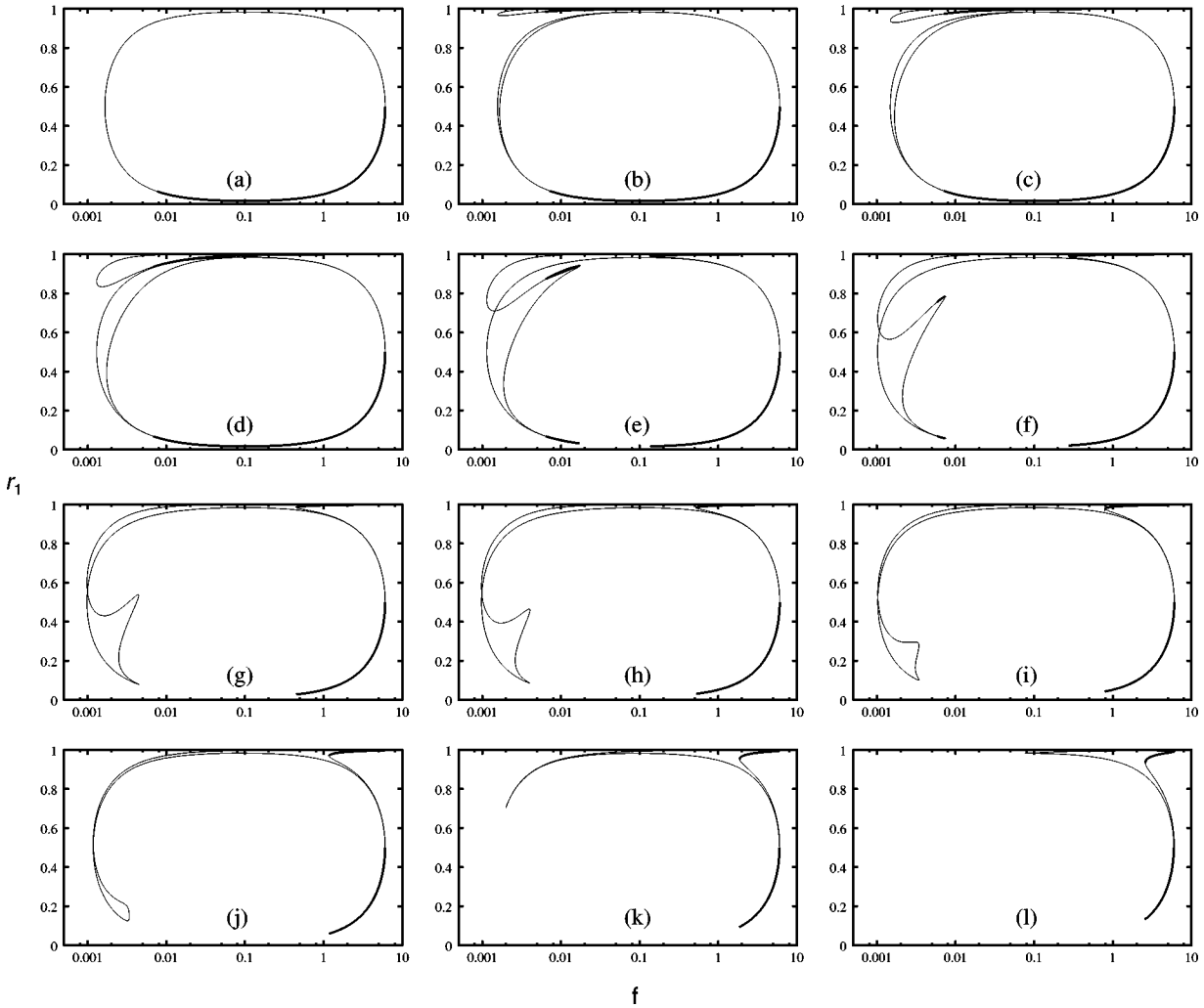

FIG. 5. Evolution of the bifurcation diagram r_1 versus f in the coupled CSTRs for changing g [Eqs. (21) and (22)] hosting a species with $k=25$ and $d=0.1$. Coupling feed rate is (a) 0, (b) 0.0001, (c) 0.0002, (d) 0.0005, (e) 0.001, (f) 0.002, (g) 0.004, (h) 0.005, (i) 0.01, (j) 0.02, (k) 0.05, and (l) 0.1. The trivial steady state at $r_1=1$ is not shown. Also for the sake of clarity, the steady states of the decoupled case only are shown in (a).

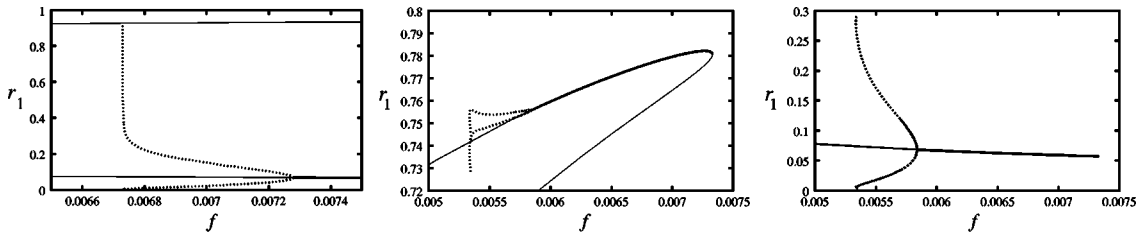

FIG. 7. Limit cycles emanating from the Hopf bifurcation points in r_1 versus f plane. The species in the environment have reproduction and death rates $k=25$ and $d=0.1$, respectively. Solid lines are steady states, while symbols represent the extrema of limit cycles.

neath the lower horizontal line shows the evolution of the limit points of the emergence isola of Figs. 3(a) and 3(b). Therefore, above the upper horizontal line (Region I), and below the lower horizontal line and the emergence limit points (Region II), the system only has the trivial steady state. Similarly, on the right-hand side of the right-most branching points curve (Region III), the system has two steady states on the single-CSTR isola, and the trivial steady state. In other words, the static structure of the coupled system is equivalent to that of a single-CSTR system, if we operate the system in Regions I, II, or III.

B. Dynamic Complexity

The system described by Eqs. (19) and (20) can have up to three Hopf bifurcations in the states versus the feed flow rate space. One of the Hopf bifurcations occurs on the symmetric steady state SS22 at the flow rate given by Eq. (30), since the bifurcation diagram of the symmetric steady states of the coupled CSTRs is identical to that of the single CSTR. The other two possible Hopf bifurcations occur on the asymmetric steady states SS02 and SS20, as they are the only possible new steady states that can develop from two stable steady states.

Example 3.: Stable steady states, limit cycles, and chaos. Let us investigate the system of Example 1, with an interaction flow rate $g=0.002$. Fig. 7 shows the limit cycles coming out of the three Hopf bifurcations. The limit cycles of Fig. 7(a) correspond to those that develop from SS22, and the ones shown in Figs. 7(b) and 7(c) develop from SS02 and SS20, respectively. Note that, the first bifurcation diagram cannot have any period doubling, as it corresponds to autonomous two-dimensional dynamics. Furthermore, numerical studies showed that, the second (hence the third) bifurcation diagram does not have any period doubling either. Yet, the system still exhibits chaotic behavior reached through quasiperiodicity. For instance, if we couple two individually oscillating CSTRs with a phase angle, the oscillations either lock into a single oscillation or result in chaos. If we perturb the system around the locked oscillation or its strange attractor, it may also converge to a stable steady state. In Fig. 8, these three scenarios are shown on the (r_1,p_1) and (r_1,r_2) projections of the phase space. In the first one, after a long transient regime, the two CSTRs get locked on the single-CSTR limit cycle [Fig. 8(a)]. The second one is a strange attractor [Fig. 8(b)], and the third one shows the stable and unstable steady states of the system, with ● and ×, respectively.

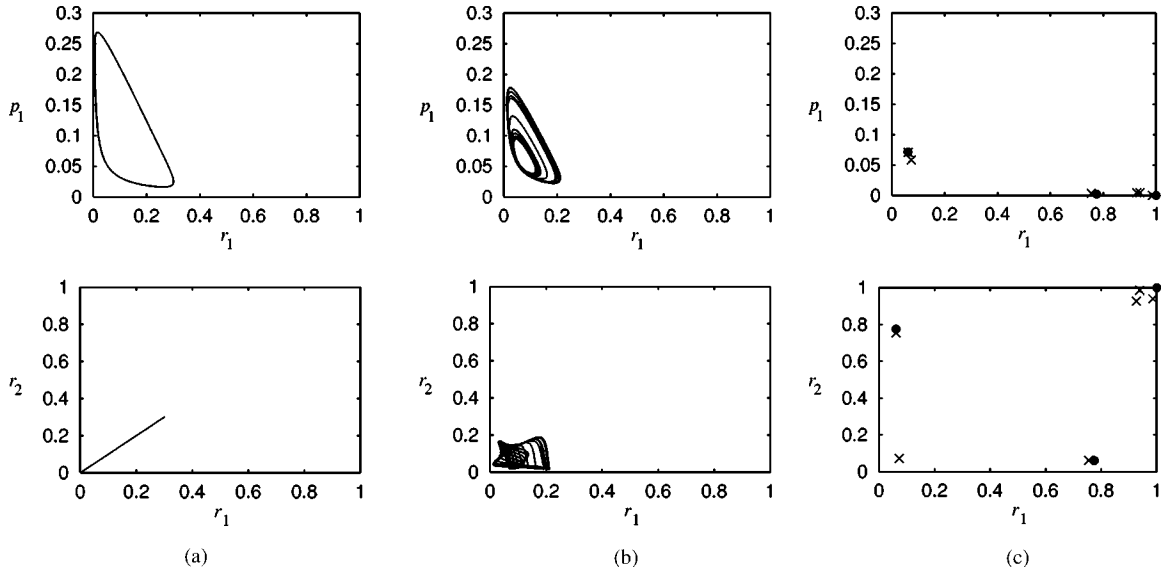

FIG. 8. Coupling two oscillating CSTRs with $f=0.006\,74$ and $g=0.002$ either (a) results in an identical limit cycle in two reactors, or (b) results in a chaotic motion, or (c) the system can go to one of its stable steady states shown with ●. For comparison we have also shown the unstable steady states of the system with ×.

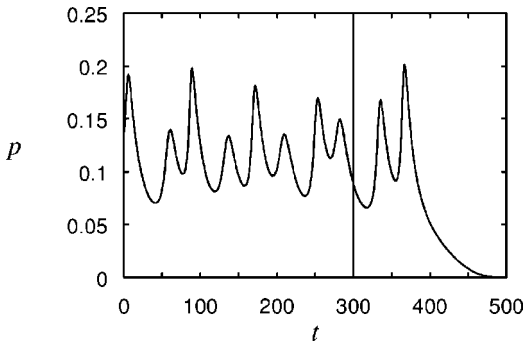

FIG. 9. Species of Example 3 in two CSTRs with a feed rate $f=0.006\,65$. Initially the CSTRs are coupled by an interaction flow rate $g=0.002$, and the interaction is removed at $t=300$.

Thus the system may have multiple stable steady states, a stable limit cycle, and multiple strange attractors (the one that is shown in Fig. 8(b) and its mirror symmetry) for the same parameter set. Accordingly, it will be attracted to either one, depending on its initial conditions. Furthermore, it can be transfered from one regime to another by small perturbations, due to the mingled nature of different basins of attraction.

Furthermore, although this species cannot have any limit cycle for $f<0.006\,728\,6$, and $g=0.002$, it does have strange attractors until $f\simeq 0.0066$. Hence, the species survives, *living* on a strange attractor manifold, and would die out if the coupling were removed. Figure 9 shows the average population of p in the system, initially on a strange attractor for a feed rate $f=0.006\,65$ and an interaction flow rate $g=0.002$. After the interaction flow is removed at $t=300$, the P concentrations in both CSTRs go to zero. This illustrates another type of emergence in the coupled system.

Example 4: Multiple limit cycles. Another dynamic richness of the system of a cubic autocatalytic species in two CSTRs is that, it can have a high order of limit cycle multiplicity. For example, consider the species with $k=25$ and $d=0.1$, living in two CSTRs that are fed with a flow rate $f=0.006\,729$, and interaction flow rate is $g=0.0005$. This system has five stable limit cycles, as shown in Fig. 10.

In Fig. 10(a), (r_1,p_1) and (r_1,r_2) projections of the limit cycles are shown with the stable (●) and unstable (×) steady states of the system. The limit cycle shown by a line in (r_1,r_2) projection is the limit cycle that is inherited from the single-CSTR dynamics. Figure 10(b) is the closeup of the limit cycle, centered around $r_2=0.9356$ and is seen as a line in Fig. 10(a), which shows that it does indeed oscillate in r_2, as well. The same is valid for the limit cycle centered around $r_1=0.9356$, since we have a mirror symmetry between the two CSTRs of the system. Also, note that the limit cycle shaped like a figure-eight in (r_1,r_2) projection is indeed two limit cycles with a phase difference of π on top of each other, again due to mirror symmetry. Another interesting property of this limit cycle is that, while it undergoes a single cycle in the (r_1,r_2) projection, it makes two identical cycles in the (r_1,p_1) projection.

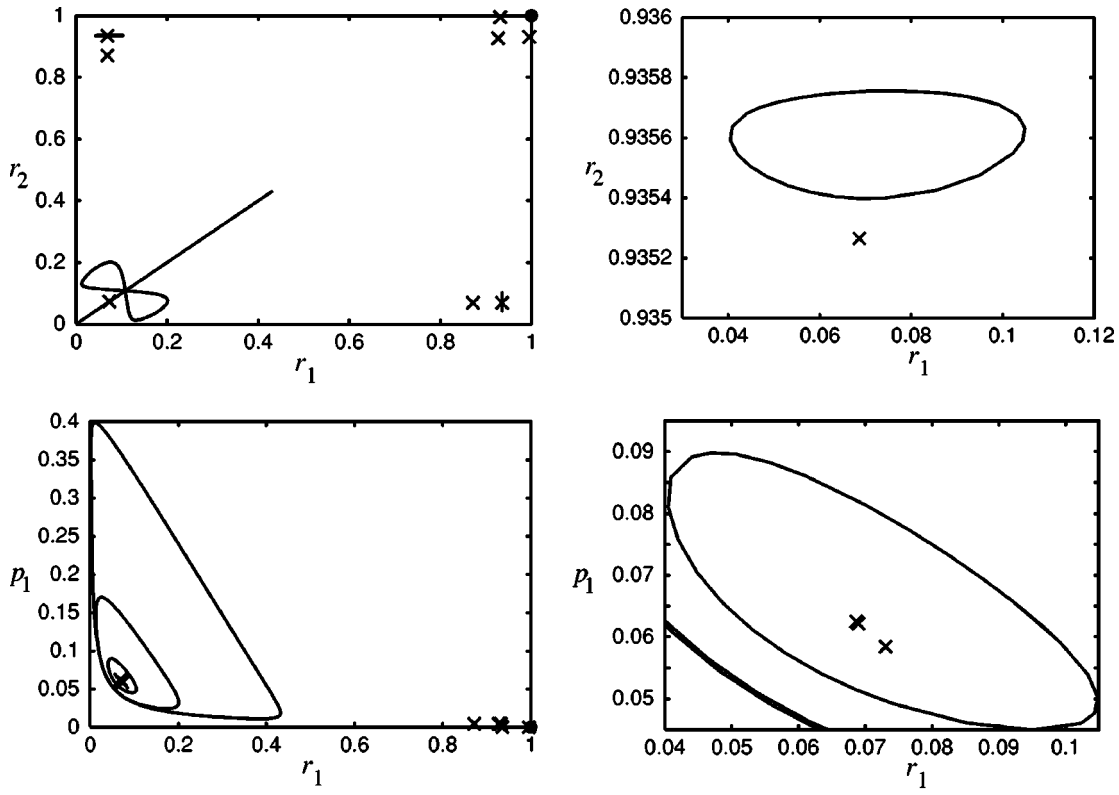

(a) (b)

FIG. 10. Multiple stable limit cycles and steady states of the system of example 4.

TABLE I. 49 steady states of a system of two CSTRs with two species P and Q of example 5 and their stability. Steady states are grouped in four sets: total extinction (1), P only (2–9), Q only (10–17), and coexistence (18–49).

	CSTR 1			CSTR 2			
SS	r_1	p_1	q_1	r_2	p_2	q_2	Stability
1	1.000×10^{0}	0.000×10^{0}	0.000×10^{0}	1.000×10^{0}	0.000×10^{0}	0.000×10^{0}	Stable
2	9.490×10^{-1}	4.636×10^{-3}	0.000×10^{0}	9.490×10^{-1}	4.636×10^{-3}	0.000×10^{0}	Unstable
3	5.100×10^{-2}	8.627×10^{-2}	0.000×10^{0}	5.100×10^{-2}	8.627×10^{-2}	0.000×10^{0}	Stable
4	9.526×10^{-1}	4.661×10^{-3}	0.000×10^{0}	9.957×10^{-1}	4.239×10^{-5}	0.000×10^{0}	Unstable
5	4.743×10^{-2}	9.361×10^{-2}	0.000×10^{0}	9.110×10^{-1}	1.085×10^{-3}	0.000×10^{0}	Stable
6	4.754×10^{-2}	9.336×10^{-2}	0.000×10^{0}	8.819×10^{-1}	3.967×10^{-3}	0.000×10^{0}	Unstable
7	9.957×10^{-1}	4.239×10^{-5}	0.000×10^{0}	9.526×10^{-1}	4.661×10^{-3}	0.000×10^{0}	Unstable
8	8.819×10^{-1}	3.967×10^{-3}	0.000×10^{0}	4.754×10^{-2}	9.336×10^{-2}	0.000×10^{0}	Unstable
9	9.110×10^{-1}	1.085×10^{-3}	0.000×10^{0}	4.743×10^{-2}	9.361×10^{-2}	0.000×10^{0}	Stable
10	8.363×10^{-1}	0.000×10^{0}	4.424×10^{-2}	8.363×10^{-1}	0.000×10^{0}	4.424×10^{-2}	Unstable
11	1.637×10^{-1}	0.000×10^{0}	2.260×10^{-1}	1.637×10^{-1}	0.000×10^{0}	2.260×10^{-1}	Stable
12	8.432×10^{-1}	0.000×10^{0}	4.503×10^{-2}	9.856×10^{-1}	0.000×10^{0}	1.224×10^{-3}	Unstable
13	1.568×10^{-1}	0.000×10^{0}	2.421×10^{-1}	9.182×10^{-1}	0.000×10^{0}	7.868×10^{-3}	Stable
14	1.578×10^{-1}	0.000×10^{0}	2.398×10^{-1}	8.089×10^{-1}	0.000×10^{0}	3.947×10^{-2}	Unstable
15	9.856×10^{-1}	0.000×10^{0}	1.224×10^{-3}	8.432×10^{-1}	0.000×10^{0}	4.503×10^{-2}	Unstable
16	8.089×10^{-1}	0.000×10^{0}	3.947×10^{-2}	1.578×10^{-1}	0.000×10^{0}	2.398×10^{-1}	Unstable
17	9.182×10^{-1}	0.000×10^{0}	7.868×10^{-3}	1.568×10^{-1}	0.000×10^{0}	2.421×10^{-1}	Stable
18	7.544×10^{-1}	5.833×10^{-3}	4.905×10^{-2}	7.544×10^{-1}	5.833×10^{-3}	4.905×10^{-2}	Unstable
19	2.456×10^{-1}	1.791×10^{-2}	1.506×10^{-1}	2.456×10^{-1}	1.791×10^{-2}	1.506×10^{-1}	Unstable
20	9.373×10^{-1}	4.736×10^{-3}	1.230×10^{-3}	8.378×10^{-1}	4.302×10^{-5}	4.532×10^{-2}	Unstable
21	9.789×10^{-1}	5.259×10^{-5}	1.345×10^{-3}	7.695×10^{-1}	5.769×10^{-3}	4.935×10^{-2}	Unstable
22	9.314×10^{-1}	4.715×10^{-3}	1.352×10^{-3}	7.646×10^{-1}	5.764×10^{-3}	4.967×10^{-2}	Unstable
23	4.830×10^{-2}	9.192×10^{-2}	1.366×10^{-3}	7.330×10^{-1}	9.898×10^{-4}	5.180×10^{-2}	Unstable
24	4.858×10^{-2}	9.135×10^{-2}	1.498×10^{-3}	6.683×10^{-1}	5.681×10^{-3}	5.682×10^{-2}	Unstable
25	5.061×10^{-2}	8.759×10^{-2}	3.802×10^{-3}	2.642×10^{-1}	1.598×10^{-2}	1.438×10^{-1}	Unstable
26	8.810×10^{-1}	4.862×10^{-3}	4.853×10^{-3}	2.320×10^{-1}	1.909×10^{-2}	1.637×10^{-1}	Unstable
27	9.279×10^{-1}	1.803×10^{-4}	4.928×10^{-3}	2.305×10^{-1}	1.926×10^{-2}	1.647×10^{-1}	Unstable
28	5.126×10^{-2}	8.661×10^{-2}	5.647×10^{-3}	1.783×10^{-1}	8.064×10^{-4}	2.130×10^{-1}	Stable
29	8.671×10^{-1}	5.120×10^{-3}	7.671×10^{-3}	1.579×10^{-1}	4.620×10^{-5}	2.405×10^{-1}	Unstable
30	7.965×10^{-1}	1.775×10^{-4}	4.297×10^{-2}	2.327×10^{-1}	1.908×10^{-2}	1.622×10^{-1}	Unstable
31	8.289×10^{-1}	5.306×10^{-5}	4.452×10^{-2}	7.614×10^{-1}	5.831×10^{-3}	4.871×10^{-2}	Unstable
32	7.286×10^{-1}	6.094×10^{-3}	4.490×10^{-2}	1.593×10^{-1}	5.501×10^{-5}	2.374×10^{-1}	Unstable
33	8.378×10^{-1}	4.302×10^{-5}	4.532×10^{-2}	9.373×10^{-1}	4.736×10^{-3}	1.230×10^{-3}	Unstable
34	7.199×10^{-1}	5.993×10^{-3}	4.815×10^{-2}	2.349×10^{-1}	1.885×10^{-2}	1.605×10^{-1}	Unstable
35	7.614×10^{-1}	5.831×10^{-3}	4.871×10^{-2}	8.289×10^{-1}	5.306×10^{-5}	4.452×10^{-2}	Unstable
36	7.695×10^{-1}	5.769×10^{-3}	4.935×10^{-2}	9.789×10^{-1}	5.259×10^{-5}	1.345×10^{-3}	Unstable
37	7.646×10^{-1}	5.764×10^{-3}	4.967×10^{-2}	9.314×10^{-1}	4.715×10^{-3}	1.352×10^{-3}	Unstable
38	7.330×10^{-1}	9.898×10^{-4}	5.180×10^{-2}	4.830×10^{-2}	9.192×10^{-2}	1.366×10^{-3}	Unstable
39	6.683×10^{-1}	5.681×10^{-3}	5.682×10^{-2}	4.858×10^{-2}	9.135×10^{-2}	1.498×10^{-3}	Unstable
40	2.642×10^{-1}	1.598×10^{-2}	1.438×10^{-1}	5.061×10^{-2}	8.759×10^{-2}	3.802×10^{-3}	Unstable
41	2.438×10^{-1}	1.821×10^{-2}	1.497×10^{-1}	1.655×10^{-1}	1.651×10^{-4}	2.256×10^{-1}	Unstable
42	2.349×10^{-1}	1.885×10^{-2}	1.605×10^{-1}	7.199×10^{-1}	5.993×10^{-3}	4.815×10^{-2}	Unstable
43	2.327×10^{-1}	1.908×10^{-2}	1.622×10^{-1}	7.965×10^{-1}	1.775×10^{-4}	4.297×10^{-2}	Unstable
44	2.320×10^{-1}	1.909×10^{-2}	1.637×10^{-1}	8.810×10^{-1}	4.862×10^{-3}	4.853×10^{-3}	Unstable
45	2.305×10^{-1}	1.926×10^{-2}	1.647×10^{-1}	9.279×10^{-1}	1.803×10^{-4}	4.928×10^{-3}	Unstable
46	1.783×10^{-1}	8.064×10^{-4}	2.130×10^{-1}	5.126×10^{-2}	8.661×10^{-2}	5.647×10^{-3}	Stable
47	1.655×10^{-1}	1.651×10^{-4}	2.256×10^{-1}	2.438×10^{-1}	1.821×10^{-2}	1.497×10^{-1}	Unstable
48	1.593×10^{-1}	5.501×10^{-5}	2.374×10^{-1}	7.286×10^{-1}	6.094×10^{-3}	4.490×10^{-2}	Unstable
49	1.579×10^{-1}	4.620×10^{-5}	2.405×10^{-1}	8.671×10^{-1}	5.120×10^{-3}	7.671×10^{-3}	Unstable

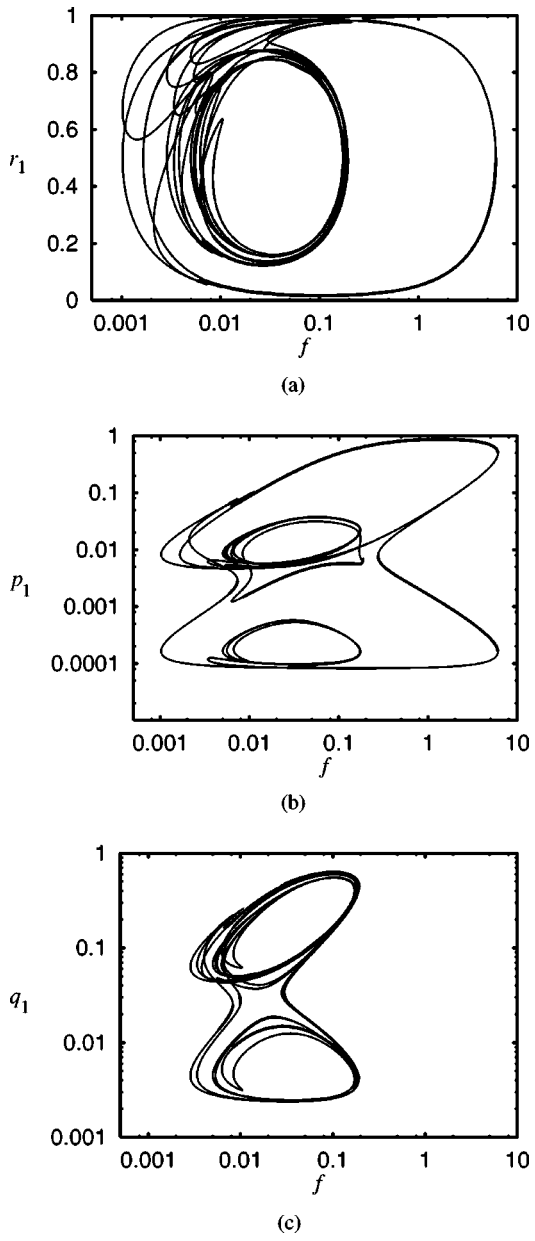

FIG. 11. Bifurcation diagram of the two species case of example 5 on (a) r_1 versus f, (b) p_1 versus f and (c) q_1 versus f planes. Note that, the latter two are drawn on a log-log scale to show detail for low level species concentrations.

IV. COEXISTENCE OF TWO SPECIES IN THE PARTITIONED ENVIRONMENT

Now, let us take a step further, and consider the coupled CSTRs when two species P and Q are allowed to populate it. The dimensionless model equations for this case are given by

$$\frac{dr_i}{dt} = -k_p r_i p_i^2 - k_q r_i q_i^2 + f(1-r_i) + g(r_{i'} - r_i), \quad (42)$$

$$\frac{dp_i}{dt} = k_p r_i p_i^2 - (f+d_p) p_i + g(p_{i'} - p_i), \quad (43)$$

$$\frac{dq_i}{dt} = k_q r_i q_i^2 - (f+d_q) q_i + g(q_{i'} - q_i), \quad (44)$$

for $i=1,2$, with $i \neq i'$, and where k_p (k_q) and d_p (d_q) are the dimensionless reproduction and death rates of species P (Q), respectively. Note that, for the two species system, the results of the single species case, investigated so far, are all valid. Namely, we still have the total extinction as a stable steady state, and there are eight additional steady states for each species. Also note that, in a single CSTR setup with two species [17] we have seven possible steady states (one for total extinction, two for each species representing partial extinction, and two for their coexistence). Again, from the implicit function theorem, we can argue that, if we start each of the two totally segregated CSTRs at one of those seven steady states, then bring the two into interaction, by slowly increasing the interaction flow rate, the steady states will evolve continuously into new steady states. Thus, for some range of $g \in (0, g_{\max})$, we may observe up to 49 steady states for this system, as illustrated by the following example.

Example 5: The steady state structure. Let us consider species P with $k_p=25$ and $d_p=0.1$ as in the previous sections, and let the second species Q be defined by $k_q=1$ and $d_q=0.027$. For a feed flow rate of $f=0.01$, and an interaction flow rate of $g=0.001$, 49 distinct steady states are possible. These have been computed and their stability characteristics determined as shown in Table I.

If we continue these 49 steady states using the feed flow rate f as our bifurcation parameter, we obtain the bifurcation diagram of Fig. 11. When compared with the P-only bifurcation diagram of Fig. 4, Fig. 11(a) reveals that the introduction of the second species increases the level of complexity of the bifurcation diagram considerably, as the maximum steady state multiplicity has increased from nine to 49. To better show the details of this, we have plotted the (f,p_1) and (f,q_1) projections of the bifurcation diagram on a log-log scale [Figs. 11(b) and 11(c), respectively]. Notice that, the trivial stable steady state of total extinction is not shown in any of the projections. For added clarity, Fig. 12 presents a breakup of this bifurcation diagram into three sets of solution curves, those supporting P only, those supporting Q only, and those where existence of both P and Q is observed. Note that, the (f,r_1) plane projection of the P-only steady states are identical to those of Fig. 4, and that those of the Q-only steady states are similar. We can clearly see from the coexistence steady states shown in Figs. 12(b), 12(e), and 12(h) that the two-CSTR system is capable of hosting two species on multiple stable steady states (for example steady states 28 and 46 of Table I, which are mirror images of each other). Another interesting point we observe in Fig. 12 is that, while the coexistence steady states form a bundle in (f,q_1) projection [Fig. 12(h)], they are grouped in three disjoint sets in (f,p_1) projection [Fig. 12(e)].

Similar to the single species analysis, we can study the effect of the interaction flow rate, g, on the bifurcation structure. If we fix the feed flow rate at $f=0.01$, we can use the interaction flow rate g to plot the bifurcation diagram of Fig. 13. We can see that the system has a pair of stable coexist-

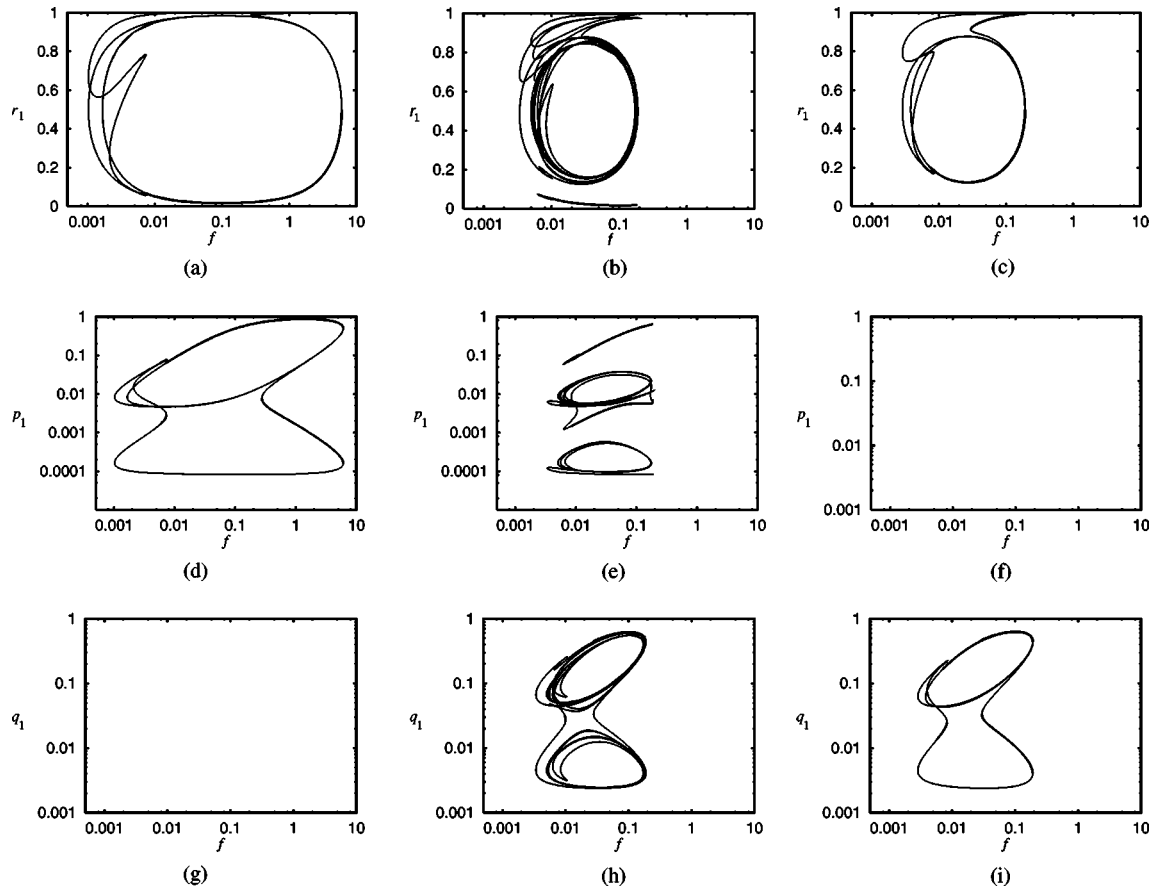

FIG. 12. Breakup of the bifurcation diagram of the two species case of example 5. (a), (b), and (c) show an r_1 versus f projection, (d), (e), and (f) show a p_1 versus f projection, (g), (h), and (i) show a q_1 versus f projection of P-only, P and Q, and Q-only steady states, respectively.

ence steady states in the range $g \in (0,0.0045)$, and roughly after $g=0.054$ the coupled CSTRs have a steady state structure identical to that of a single CSTR.

Example 6: Two species oscillation. Next, we consider some numerical experiments that explore oscillatory coupling in this system. If we totally segregate the system of the previous example and feed it with a flow rate $f=0.007$, under certain conditions, we can arrange a setup where the first CSTR has an oscillating species P, and the second CSTR has an oscillating species Q [Fig. 14(a)]. Next, we can couple the two CSTRs with certain interaction flow rate and observe the effect of coupling. Depending on the timing and the strength of coupling, the system can go to a two species quasiperiodic oscillation [Fig. 14(b)]; to a setup where one of the CSTRs is dominated by an oscillating P, and Q is gone extinct [Fig. 14(c)]; to a setup where one of the CSTRs is dominated by P at steady state, and Q is gone extinct [Fig. 14(d)]; to a setup where both of the CSTRs are dominated by an oscillating P, and Q is gone extinct [Fig. 14(e)]; or to a total extinction steady state [Fig. 14(f)]. Note that, the oscillations shown in Fig. 14(b) are actually quasiperiodic oscillations, which is evident from the concentration fluctuations of p_1 and q_2, shown in Fig. 15. Also note that, the last two cases shown in Figs. 14(e) and 14(f) have the same interaction flow rate, yet exhibit different type of final behavior, due to the timing of the coupling.

Example 7: Two species chaos. Numerical studies performed suggest that, two species can coexist in two identical CSTRs either at a steady state, or on a quasiperiodic attractor. Although theoretically, it may still be possible to sustain coexistence on a chaotic attractor in the two identical CSTRs setup studied, our numerical analysis could not locate such behavior in the range of parameters considered. To push the quasiperiodic regime into a full-fledged chaos, we needed to either relax the identical CSTRs condition, or increase the level of partitioning by considering a three-CSTR setup.

To that end, let us first consider three CSTRs hosting two species, P with $k_p=24$ and $d_p=0.1$, and Q with $k_q=24.5$ and $d_q=0.099$. If we operate the system of totally segregated CSTRs with a feed flow rate $f=0.007$, both of the species will have stable limit cycle regimes. Now, we start the system with seeding the first CSTR with Q, and the second and the third with P. After they reach their stable limit cycle, if we connect the three with an interaction flow rate $g=0.0005$, in the resulting system we will have the first CSTR dominated by Q, and other two dominated by P, and the limit cycle of the species will evolve into a strange attractor. Figure 16 shows the concentration of the dominant species versus the resource concentration in each tank.

Alternatively, let us relax the condition of identical CSTRs, and consider a two-CSTR system with the second CSTR having a volume that is twice that of the first one, and

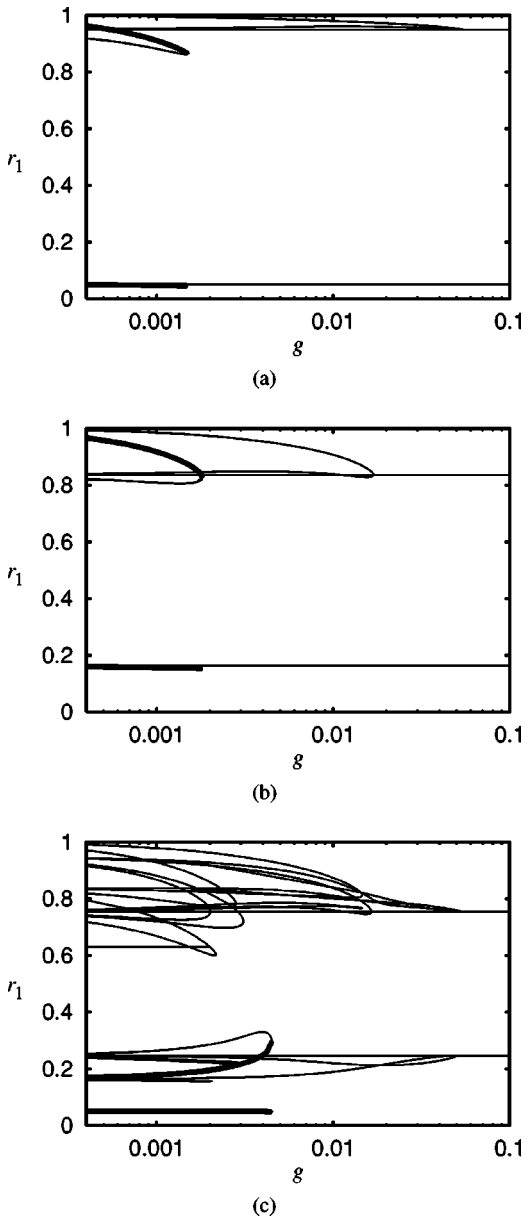

FIG. 13. Bifurcation diagram of the two species case of example 5, on r_1 versus g plane. (a) P only, (b) Q only and (c) coexistence steady states.

is fed with a flow rate that is twice that of the first. If we seed this system with the same species P and Q as above, and operate the system with $f=0.007$ and $g=0.0005$, in operating conditions of Fig. 17, the first CSTR will be dominated by Q, and other one dominated by P. Thus, the two species will again be able to coexist on a strange attractor.

V. CONCLUSIONS

This article analyzes the effect of environmental partitioning on the survival fate of multiple cubic autocatalytic replicators that inhabit this environment, and compete for a common resource. The partitioned environment was modeled as two coupled CSTRs. Analysis showed that the steady states of the decoupled system, which are also present in the coupled case, conserve their stability structure after coupling. For the case of a single species, we investigated the mechanism by which new steady states develop in the coupled system. A continuation study on the new steady states revealed that, the coupled system may have survival steady states, where the decoupled system cannot. Thus, we witness emergence of new (albeit unstable) steady states due to the complexity offered by coupling. Another encounter with emergence phenomena occurred in the parameter range, where the decoupled system did not have any stable survival steady states. The coupled system, this time, expanded the range of stability for the survival of the species. In one of the environments, we had high concentration of the species—in fact, higher than the (unstable) steady states of the decoupled system can reach—and in the other we had a lower concentration. A third kind of emergence phenomenon occurred next to the limit cycle regime of the decoupled system, which is also valid for the coupled case. When the limit cycle of the decoupled system ceased to exist, the coupled system enjoyed a strange attractor. Once more, the species survived where it would not, should the coupling be removed.

Theoretical and experimental studies suggest that, coexistence of pure and simple competitors in a homogeneous environment with uniform feed flow rate is not possible. We have shown that the autocatalytic replicators setup is in agreement with this, so called, competitive exclusion principle. One remedy of this is to partition the environment. In this work we have shown the mathematical reasoning of why and how partitioning brings the possibility of coexistence. We also conjecture that the number of steady states of multiple species living in a partitioned environment increases exponentially both with the number of species and the number of partitions. Results demonstrate that, stable coexistence of two species is impossible in this environment, in a multitude of configurations. These include steady state, periodic and quasiperiodic attractors as well as chaotic attractors.

The two-CSTR system considered here is an example of two well-mixed subsystems interconnected via two-way exchange of living species (autocatalysts) P and Q and nutrient resource R. With resource introduced via feed devoid of autocatalysts and loss of both autocatalysts and resource via the effluent in each subsystem, the two-reactor system is representative of the industrial scale biological production processes and biological waste treatment processes. The rates of exchange of P, Q, and R between the two subsystems are proportional to the differences in concentrations of the respective species in the two subsystems and are therefore, representative of diffusive transport between the subsystems. Segregation of a system into two or more subsystems based on spatial inhomogeneity, with exchange of one or more species occurring between the subsystems by diffusion, has been shown to lead to coexistence of two competing living species under conditions where such coexistence would not be permissible if the system were spatially homogeneous [16,26,35–37]. It is well known that diffusive transport enables coexistence of competing living species both in mechanochemical systems (such as that considered here) and ecological systems [16].

Although the focus of this article is on a two-CSTR sys-

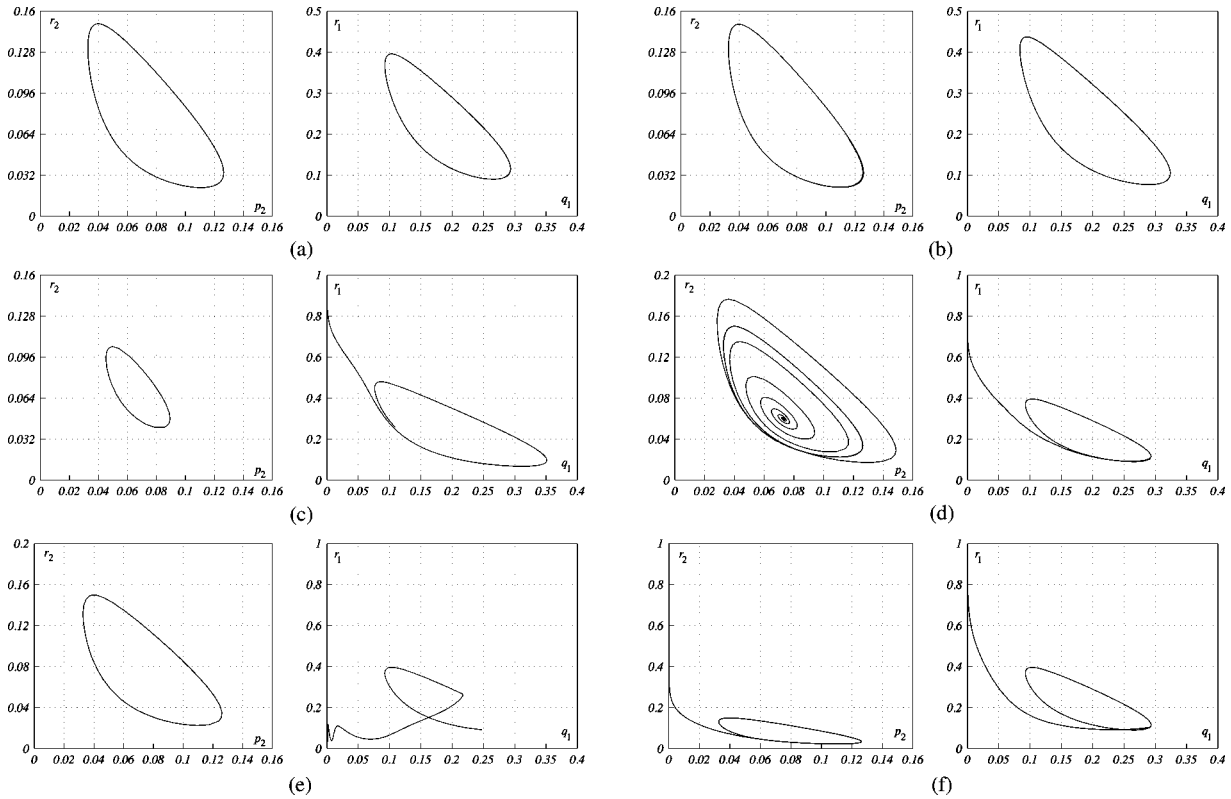

FIG. 14. (a) Two separate oscillating CSTRs with species P in one and species Q in the other, can go to (b) a coupled oscillation for $g=0.000\,02$, (c) a P-dominated oscillation in one reactor with Q gone extinct for $g=0.0002$, (d) a P-dominated steady state in one reactor with Q gone extinct for $g=0.002$, (e) a P dominated identical oscillation in both reactors with Q gone extinct for $g=0.04$, and (f) a total death for $g=0.04$.

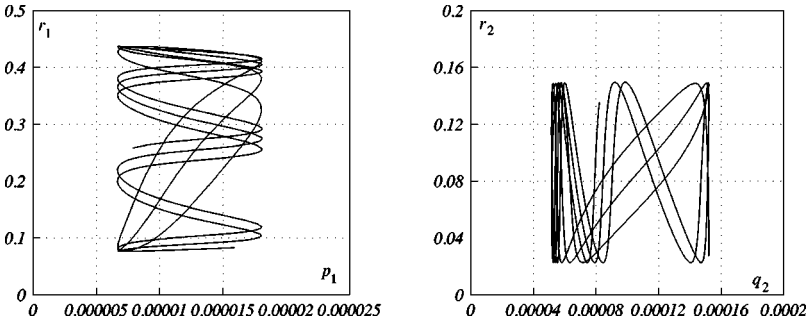

FIG. 15. Concentrations of (a) P in the first CSTR, and (b) Q in the second CSTR versus the resource concentration in the respective CSTR for the two-species oscillation of Fig. 14(b).

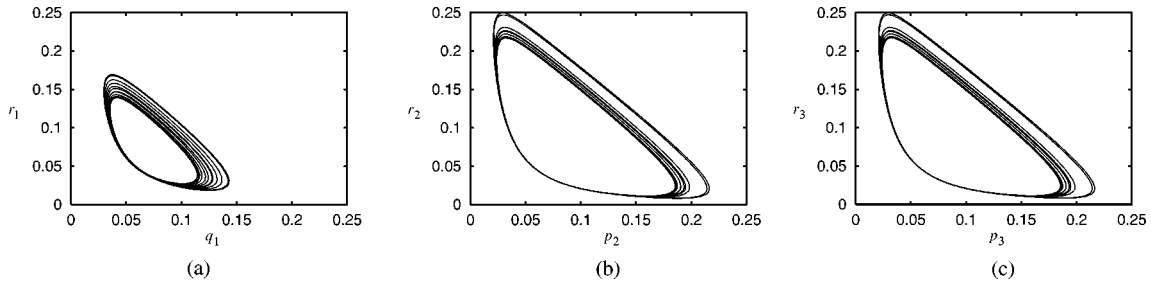

FIG. 16. Concentrations of (a) Q in the first CSTR, (b) P in the second CSTR, and (c) P in the third CSTR, versus the resource concentration in the respective tank for the three CSTRs of example 7.

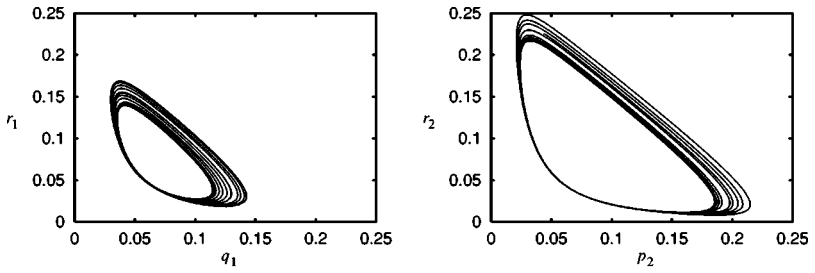

FIG. 17. Concentrations of (a) Q in the first CSTR, and (b) P in the second CSTR, versus the resource concentration in the respective tank for the two CSTRs of example 7.

tem, the approach undertaken here can be readily extended to several interconnected (via diffusive transport) CSTRs, thereby allowing one to mimic ecological systems as composites of several discrete reaction-diffusion systems. The extension would of course involve modification of certain terms in Eqs. (3)–(6) and Eqs. (42)–(44), which are reflective of reactors operated by humans in industrial settings. For example, the source term for R, in general, will not be spatially uniform, and may involve temporal variations. In the case of ecological systems, each subsystem can be represented by a well-mixed reactor accounting for reproduction and death of each living species, resource utilization, resource generation (supply) and diffusive exchange of living species and resource between subsystems. One can argue that, the terms reflecting the loss of resource and populations via reactor effluent would be absent, with few exceptions, in representation of ecological systems. An example exception is description of events in large lakes and rivers. These systems can be subdivided into subsystems based on variation in flow rate with depth. The subsystem comprised of section at the bottom would essentially be stagnant (thus $f_{\text{bottom}}=0$), while the subsystem comprised of the top section near the air-water interface would have the highest flow rate ($f_{\text{top}}>0$). The mathematical representation in this situation should account for loss of resource and populations via subsystem effluent with distinct flow rates in different subsystems.

Also note that, in the mathematical description of the system, death process, characterized by d_i for species i, always appears in an additive form with the physical loss of species, characterized by f. Thus, one can in principle lump the two processes into $D_i=d_i+f$, and reformulate the model equations using parameters k_i, D_i, and f, instead of k_i, d_i, and f. Although doing so would impose certain restrictions on the magnitudes of the individual parameters, the analyses presented in this work will stay intact in this constrained parameter space.

As a result, the cubic autocatalytic replicators in partitioned environments scheme is apt for the investigation of mathematical ecologies. Even a single species in two coupled environments introduces the type of complex behavior we expect to see in the natural and artificial ecologies. It is further demonstrated that, the most important effect of environment partitioning, as far as mathematical ecologies are concerned, is that, it enables stable static and dynamic coexistence of multiple autocatalytic replicators. Moreover, it is possible to relax the assumption of identical CSTRs, and preliminary results suggest increasing complexity by, e.g., allowing different flow rates for different CSTRs.

[1] J.E. Bailey and D.F. Ollis, *Biochemical Engineering Fundamentals* (McGraw-Hill, New York, 1977).
[2] H.R. Bungay and M.L. Bungay, Adv. Appl. Microbiol. **10**, 269 (1968).
[3] p. Gray and S.K. Scott, Chem. Eng. Sci. **39**, 1087 (1984).
[4] R.S. Li and H.J. Li, Chem. Eng. Sci. **44**, 2995 (1989).
[5] R.S. Li, Chem. Eng. Sci. **49**, 2029 (1994).
[6] F.P. Stadler, W. Schnabl, C.V. Forst, and P. Schuster, Bull. Math. Biol. **57**, 21 (1995).
[7] S. Focant and T. Gallay, Physica D **120**, 346 (1998).
[8] P. Schuster and W. Fontana, Physica D **133**, 427 (1999).
[9] M. Eigen and P. Schuster, *The Hypercycle: A Principle of Natural Self-Organization* (Springer-Verlag, Berlin, 1979).
[10] D.J. Smith, S. Forrest, D.H. Ackley, and A.S. Perelson, Bull. Math. Biol. **60**, 647 (1998).
[11] R.J.D. Boer and A.S. Perelson, J. Theor. Biol. **190**, 201 (1998).
[12] V.A.A. Jansen and K. Sigmund, Theor Popul. Biol. **54**, 195 (1998).
[13] R.K. Standish, *Ecolab: Where to Now?* (IOS, Amsterdam, 1996), pp. 262–271.
[14] P.F. Stadler and R. Happel, J. Math. Biol. **38**, 422 (1999).
[15] L. Edelstein-Keshet, *Mathematical Models in Biology* (Random House, New York, 1988).
[16] J.D. Murray, *Mathematical Biology* (Springer-Verlag, Berlin, 1993).
[17] I. Birol and F. Teymour, Physica D **144**, 279 (2000).
[18] G. Birol, A.-Q.M. Zamamiri, and M.A. Hjortsø, Process Biochemistry **10**, 1085 (2000).
[19] G. Hardin, Science **131**, 1292 (1960).
[20] G.E. Hutchinson, Am. Nat. **95**, 137 (1961).
[21] P.G. Risser, J. Lubchenco, and S.A. Levin, BioScience **41**, 625 (1991).
[22] A.G. Fredrickson and G. Stephanopoulos, Science **213**, 972 (1981).
[23] P. Gray and S.K. Scott, Chem. Eng. Sci. **38**, 29 (1983).
[24] K.I. Alhumaizi and A.E. Abasaeed, Chem. Eng. Sci. **55**, 3919 (2000).
[25] *Santa Fe Institute Studies in the Science Series*, edited by D. Pines, G.W. Cowan, and D. Meltzer (Perseus, Cambridge, 1999), Vol. 19.

[26] S. Pavlou, I.G. Kevrekidis, and G. Lyberatos, Biotechnol. Bioeng. **35**, 224 (1990).
[27] A.G. Fredrickson and H.M. Tsuchiya, *Microbial Kinetics and Dynamics* (Prentice Hall, Englewood Cliffs, 1977), pp. 405–483.
[28] S.W. Chang and B.C. Baltzis, Biotechnol. Bioeng. **33**, 460 (1989).
[29] B.C. Baltzis and A.G. Fredrickson, Biotechnol. Bioeng. **25**, 2419 (1983).
[30] I. Barradas and K. Tassier, J. Math. Biol. **39**, 518 (1999).
[31] M. Dixon and E.C. Webb, *Enzymes*, 3rd ed. (Academic Press, New York, 1979).
[32] J. Monod, Ann. Inst. Pasteur (Paris) **79**, 390 (1950).
[33] M.L. Shuler and F. Kargi, *Bioprocess Engineering: Basic Concepts* (Prentice Hall, Englewood Cliffs, 1992).
[34] J. Nielsen and J. Villadsen, *Bioreaction Engineering Principles* (Plenum Press, New York, 1994).
[35] G. Stephanopoulos, A.G. Fredrickson, and R. Aris, AIChE J. **25**, 863 (1979).
[36] G. Stephanopoulos and A.G. Fredrickson, Biotechnol. Bioeng. **21**, 1491 (1979).
[37] B.C. Baltzis and M. Wu, Math. Biosci. **123**, 147 (1994).
[38] S.J. Parulekar and H.C. Lim, Chem. Eng. Sci. **41**, 2605 (1986).
[39] S.J. Parulekar and H.C. Lim, Chem. Eng. Sci. **41**, 2617 (1986).
[40] J. Lee and S.J. Parulekar, Chem. Eng. Sci. **51**, 217 (1996).
[41] W. Chaivorapoj, Master's thesis, Illinois Institute of Technology, 2001 (unpublished).
[42] W. Chaivorapoj, I. Birol, and F. Teymour, Ind. Eng. Chem. Res. **41**, 3630 (2002).
[43] E. Ott, *Chaos in Dynamical Systems* (Cambridge University Press, Cambridge, 1993).
[44] S.H. Kim and V. Hlavacek, Chem. Eng. Sci. **41**, 2767 (1986).
[45] M.A. Taylor and I.G. Kevrekidis, Physica D **51**, 274 (1991).
[46] M.A. Taylor and I.G. Kevrekidis, Chem. Eng. Sci. **48**, 2129 (1993).
[47] *Maple V Release 5* (Waterloo Maple Inc., Ontario, 1998).
[48] Y.A. Kuznetsov and V.V. Levitin, *A Multiplatform Environment for Analyzing Dynamical Systems* (Dynamical Systems Lab., Centrum voor Wiskunde en Informatica, Amsterdam, 1996).
[49] M.F. Kinnaird, *International Wildlife*, July/August 1997.